

# Molecular Design Using Signal Processing and Machine Learning: Time-Frequency-*like* Representation and Forward Design

Alain B. Tchagang, *Member, IEEE*, Ahmed H. Tewfik, *Fellow, IEEE*,  
and Julio J. Valdés, *Senior Member, IEEE*

**Abstract**—The availability of huge molecular databases generated by first principles quantum mechanics (QM) computations opens new venues for data science to accelerate the discovery of new molecules, drugs, and materials. Models that combine QM with machine learning (ML) known as QM↔ML models have been successful in delivering the accuracy of QM at the speed of ML. In this study, we show that by integrating well-known signal processing (SP) techniques (i.e. short time Fourier transform, continuous wavelet analysis and Wigner-Ville distribution) in the QM↔ML pipeline, we obtain a powerful machinery (QM↔SP↔ML) that can be used for representation, visualization and forward design of molecules. More precisely, in this study, we show that the time-frequency-*like* representation of molecules encodes their structural, geometric, energetic, electronic and thermodynamic properties. This is demonstrated by using the new representation in the forward design loop as input to a deep convolutional neural networks trained on first principles computational QM calculations such as density functional theory, which outputs the properties of the molecules. Tested on the QM9 dataset (composed of 133,855 molecules and 19 properties), the new QM↔SP↔ML model is able to predict the properties of molecules with a mean absolute error (MAE) below acceptable chemical accuracy (i.e. MAE < 1 kcal/mol for total energies and MAE < 0.1 ev for orbital energies). Furthermore, the new approach performs similarly or better compared to other ML state-of-the-art techniques described in the literature. In all, in this study, we show that the new QM↔SP↔ML model represents a powerful technique for molecular forward design, and open new venues for SP practitioners to participate in the molecular design endeavors. All the codes and data generated and used in this study are available at <https://github.com/TABeau/QM-SP-ML>.

**Index Terms**—Convolutional Neural Networks, Coulomb Matrix, Density Functional Theory, Discrete Fourier Transform, Forward Design, Inverse Design, Machine Learning, Molecules, Molecular Design, Molecular Representations, Molecular Visualization, Quantum Mechanics, Signal Processing, Scalogram, Spectrogram, Short Time Fourier Transform, Schrödinger Equations, Time-Frequency Transformation, Continuous Wavelet Transform, Wigner-Ville Distribution.

This work was supported by the National Research Council of Canada, Under the AI4D Program.

A. B. Tchagang is with the Digital Technologies Research Centre, National Research Council of Canada, 1200 Montréal Road, Ottawa, ON, K1A 0R6 Canada (e-mail: alain.tchagang@ nrc-cnrc.gc.ca).

## I. INTRODUCTION

THE objective of molecular design (MD) for new drugs and materials is to be able to generate new molecules with targeted properties, which are strategic to the innovation and progress of many chemical, agrochemical and pharmaceutical industries. One of the major challenges consists of making quantitative estimates in the chemical compound space (CCS) at moderate computational cost (milliseconds per compound or faster) [1]. Computational QM derived from first principles has traditionally been used for the discovery and design of de-novo molecules and for the study of their structures and properties. These high level quantum-chemistry calculations, may take days per molecule depending on property and system, and have chemical accuracy of 1 kcal/mol for total energies and 0.1 ev for orbital energies required for computational MD [2]-[3]. These accuracies are considered plainly satisfactory by the chemical community.

The availability of huge molecular databases [4]-[7] derived from QM computations first principles such as Density Functional Theory (DFT<sub>QM</sub>) has given rise to new methods based on machine learning (ML) [8]-[44]. These QM↔ML models have shown great promises, approaching the same accuracy as first principle QM computations at a much lower computational cost. One of the central questions in QM↔ML is how to represent molecules in a way that makes prediction of molecular properties feasible and accurate [8]. This question has already been extensively discussed in the cheminformatics and quantitative structure property relationships (QSPRs) literature, and many so-called molecular descriptors have been proposed [45]. Unfortunately, they often require a substantial amount of domain knowledge and engineering. Furthermore, they are not necessarily transferable across the whole CCS [1].

In this paper, we follow a more direct approach introduced in [8], and adopted by several other authors [1]-[2]. We learn the forward mapping between molecules and their properties from scratch using the Coulomb matrix (CM) as molecular descriptor [8]. The CM is directly derived from the geometry representation of molecules and has been shown to be invariant

A. H. Tewfik is with the Electrical and Computer Engineering Department, University of Texas at Austin, Austin, TX 78712 USA, (e-mail: tewfik@austin.utexas.edu).

J. J. Valdés is with the Digital Technologies Research Centre, National Research Council of Canada, 1200 Montréal Road, Ottawa, ON, K1A 0R6 Canada (e-mail: julio.valdes@ nrc-cnrc.gc.ca)

to translation and rotation but not to permutations or re-indexing of the atoms. Methods to tackle this issue have also been addressed. Examples include Coulomb sorted Eigen-spectrum [2], Coulomb sorted L2 norm of the matrix's columns [9], Coulomb bag of bonds [12], and random Coulomb matrices [1]. Each Coulomb sorted Eigen-spectrum or Coulomb sorted L2 norm of the matrix's columns is a 1-dimension (1D) order numerical sequence representation of a molecule. From the signal processing (SP) perspective, it can be treated as a 1D signal. SP has a long tradition and its techniques have been successfully applied to preprocess, transform, analyze and extract useful information from a wide variety of signals: static and dynamic, discrete and continuous, stationary and non-stationary. Its range of application covers a broad variety of disciplines such as engineering, biology, physiology, medicine, geology, astronomy, economics, and social sciences [45].

Here, we explore a new representation of molecules based on the aforementioned 1D signal (Eigen-spectrum) derived above. The 1D signal is transformed into a time-frequency-*like* (TFL) representation using techniques such as Short Time Fourier Transform (STFT), Continuous Wavelet Transform (CWT) and Wigner-Ville distribution (WVD). We show that these 2D TFL representation of molecules encode their structural, geometric, energetic, electronic and thermodynamic properties. This is demonstrated in this study by using the new TFL representation in the molecular forward design framework as input to a (deep) convolutional neural networks (CNN) trained on DFT<sub>QM</sub> calculations, which outputs the properties of the molecules. Tested on the QM9 dataset (a set of 133,855 molecules and 19 properties), the new QM $\leftrightarrow$ SP $\leftrightarrow$ ML model is able to predict the total energies of molecules with a mean absolute error (MAE)  $\ll 1$  kcal/mol, and orbital energies with MAE  $\ll 0.1$  eV, which are both below acceptable chemical accuracy. Our results also show that the new QM $\leftrightarrow$ SP $\leftrightarrow$ ML model performs similarly or better compared to other ML state-of-the-art techniques described in the literature. In all, in this study, we show that QM $\leftrightarrow$ SP $\leftrightarrow$ ML represents a powerful technique for molecular forward design.

The rest of this paper is organized as follows. Section II provides a background on QM. Section III provides a background on the forward MD using ML. Section IV describes the QM9 dataset used in this study. Section V deals with the CM and the 1D representation of molecules. Section VI presents the TFL representation of molecules. Section VII introduces the CNNs for mapping the TFL representations to molecular properties. Section VIII presents the results and discussions. This is followed by the conclusions in Section IX.

## II. QUANTUM MECHANICS

Quantum mechanics (QM) is the science that deals with the behavior of matter and light at the atomic and subatomic scales. The Schrödinger equation (SE) is the fundamental equation of physics for describing QM systems.

$$H\Psi(r) = E\Psi(r) \quad (1)$$

where,  $\Psi$  is the state vector of the quantum system (wave function),  $E$  is the energy eigenvalue,  $H = \frac{-\hbar^2}{2m}\nabla^2 + V(r)$  is the

Hamiltonian,  $\hbar = h/2\pi$  is the reduced Plank constant,  $m$  is the particle's mass,  $V(r)$  is the potential energy,  $r$  is the positional coordinates, and  $\nabla$  is the Laplacian operator [46]. This version corresponds to the time-independent SE. It is a partial differential equation (PDE), which uses the concept of energy conservation (Kinetic Energy + Potential Energy = Total Energy) to obtain information about the behavior of an electron bound to a nucleus. It does this by allowing an electron's wave function,  $\Psi$ , to be calculated. Solving the SE gives us  $\Psi$  and  $\Psi^2$ . With these, we get the quantum numbers and the shapes and orientations of the orbitals that characterize electrons in an atom or molecule. In other words, the SE account for the properties of molecules, atoms and their constituents (electrons, protons, neutrons, etc.)

As mentioned, by solving the SE analytically or by numerical approaches, one obtains the wave function  $\Psi$  and energy  $E$ , which allow for calculation of many properties of systems. So why are not more problems in materials science, organic chemistry, drug design, or biochemistry solved computationally? It turns out that analytically, you can only solve the SE for nuclei with one electron (e.g. H, He<sup>+</sup>, Li<sup>2+</sup>, Be<sup>3+</sup>, B<sup>4+</sup>, C<sup>5+</sup>, etc.) For all other atoms, ions, and molecules, a major problem is the computational effort required, which grows with the system size. For example, the benzene molecule (C<sub>6</sub>H<sub>6</sub>) consists of 12 nuclei and 42 electrons. The SE, which must be solved to obtain the energy and  $\Psi$  of this molecule, is a PDE in 162 variables. As pointed out in early last century by Paul Dirac, this situation requires approximate solutions in an accuracy versus generality trade-off in order to achieve computational efficiency [47]. Many such approximations were developed from both a conceptual level, such as the Born-Oppenheimer approximation, and a numerical level [48]-[57]. They lead to a variety of approaches for approximately solving the SE presented in **Table I**.

TABLE I  
HIERARCHY OF NUMERICAL APPROXIMATIONS TO SCHRODINGER'S EQUATION

Abbrev	Method	Runtime	Ref
CISDTQ	Configuration Interaction (up to quadruple excitations)	$O(N^{10})$	[48]
CC	Coupled Cluster (CCSD(T))	$O(N^7)$	[49]
CISD	Configuration Interaction (single and double excitations)	$O(N^5)$	[50]
MP2	Moller-Olesset second-order perturbation theory	$O(N^5)$	[51]
QMC	Quantum Monte Carlo	$O(N^{13}) - O(N^4)$	[52]
HF	Hartree-Fock	$O(N^3) - O(N^4)$	[53]
DFT	Density Functional Theory (Kohn-Sham)	$O(N^3)$	[55]
TB	Tight Binding	$O(N^2)$	[56]
MM	Molecular Mechanics	$O(N^2)$	[57]

Runtimes (scalings) have illustrative character, and can depend on implementation. Note that Landau  $O(\cdot)$  notation describes asymptotic behavior for  $N \rightarrow \infty$  only.  $N$  is the system size, e.g., number of atoms, electrons, or basis functions.

To clarify the differences and complexities in asymptotic runtime of methods in **Table I**, consider doubling a system's size  $N$ : For a configuration interaction and coupled cluster method with runtime  $O(N^{10})$  and  $O(N^7)$ , runtime increases by a factor of  $2^{10} = 1024$  and  $2^7 = 128$  respectively, whereas for a DFT<sub>QM</sub> and molecular mechanics methods with runtime  $O(N^3)$  and  $O(N^2)$  it increases only by a factor of 8 and 4 respectively. Even so, after a few doublings one is bound to run out of computing resources. So what to do when one requires the accuracy and wide applicability of higher level QM methods for a large system, or, a large number of small systems? Linear-

scaling QM methods might offer an alternative by exploiting locality for an excellent  $O(N)$  asymptotic runtime, but are not applicable to all systems [8, 57]. Another strategy is to use ML for its high speed and potential for accurately approximate QM solutions [8].

### III. QUANTUM MECHANICS $\leftrightarrow$ MACHINE LEARNING MODELS

The ultimate goal in  $\text{QM} \leftrightarrow \text{ML}$  is to develop surrogate models that has the same accuracy as the SE and the high speed of ML. For example, obtaining atomization energies of molecules by solving the SE is computationally very expensive. As a consequence, only a fraction of the molecules in the CCS have been characterized or labelled from a ML perspective. By training a ML algorithm on the few labelled ones, the trained  $\text{QM} \leftrightarrow \text{ML}$  model can be used to predict the atomization energy of unseen (not included in the training set) molecules. There are two types of problem in MD and ML: The forward and the inverse design. Mathematically, the forward design can be formulated as follows. Given a molecule, find its properties:

$$\text{Properties} = f(\text{Molecule}) \quad (2)$$

Conversely, the inverse design can be defined as follows: given the desired/targeted properties, find the molecules:

$$\text{Molecules} = f^1(\text{properties}). \quad (3)$$

Our focus in this study is on the forward design. The inverse design from a SP perspective will be the subject of a subsequent paper. The function  $f$  in the equations above represents the relationship between the molecules and their properties, and it is inferred during the ML training step using a set of well-labelled pairs of (molecules  $\rightarrow$  properties) referred to as the training set. Several ML techniques have been proposed in the literature to tackle the forward design problem.

TABLE II

MEAN ABSOLUTE ERRORS FOR ATOMIZATION ENERGIES  $U_0$  IN KCAL/MOL, HOMO AND LUMO ENERGIES IN ELECTRON VOLT (EV)

Ref	ML Method/Descriptor	Training-Test-sizes	$U_0$	HOMO	LUMO
[25]	EN/CM	(CV 118k-13k)	21.0	0.34	0.63
[25]	EN/BoB	(CV 118k-13k)	13.9	0.28	0.52
[25]	KRR/CM	(CV 118k-13k)	3.0	0.13	0.18
[25]	KRR/BoB	(CV 118k-13k)	1.5	0.09	0.12
[25]	KRR/BAML	(CV 118k-13k)	1.2	0.09	0.12
[27]	GPR/SOAP-GAP	(100k-31k)	0.28	-	-
[30]	NMP NN	(120k-10k)	0.49	0.04	0.04
[33]	Multitask NN	(119k-13k)	44.0	0.38	0.63
[31]	SchNet NN	(CV 110K-20K)	0.32	0.04	0.03
[34]	HIP-NN	(CV 110K-20K)	0.26	-	-
[35]	HDNN	(CV 100K-30K)	0.41	-	-
[38]	KRR/SOAP	(CV 100K-30K)	0.14	-	-
[14]	PhysNet NN	(CV 110K-20K)	0.14	-	-
[44]	MEGNet	(CV 110K-20K)	0.28	0.04	0.04

The reported MAE values correspond to scores on test sets (a random sample of the dataset unseen during training) generally after cross validation (average over different runs with different subsets of data).

**Table II** lists some of these methods and their performance on the QM9 dataset relative to 3 properties ( $U_0$ , LUMO and HOMO). As can be observed, during the past decades, ML has

been used to model total molecular energies and the HOMO/LUMO energies, among other molecular properties. ML techniques used to achieve the results described in **Table II** includes: Kernel ridge regression (KRR) [8, 9], Gaussian Process regression (GPR) [25], and Elastic Net (EN) [27, 28]. These approaches have been used on the QM7 [8-9] and QM9 datasets, and shown that when their parameters are well-tuned they can almost reach chemical accuracy for the three properties with descriptors like the Coulomb matrix (CM), bag of bonds (BoB) or the bonds angles machine learning (BAML) [24, 25]. Alongside with kernel methods, several Neural Networks (NN) have been proposed and tested for the prediction of energetic and electronic properties of QM9. Complex NN architectures have been carefully designed to achieve good predictive performances. A framework called Message Passing Neural Networks (MPNNs) that shares common attributes of several promising existing NN models for graph structured data and uses bond type features in addition to interatomic distances was proposed in [30]. It achieved exciting performances on QM9 benchmark where 11 out of 13 properties were predicted within chemical accuracy (1 kcal/mol on total energies and 0.1 eV for orbital energies). Another study was a NN engine for molecular energies called ANI, representing transferable NN potentials and utilizing a Behler and Parrinello symmetry functions to build single-atom atomic environment vector [29]. ANI was shown to predict total molecular energies at the level of  $< 1.5$  kcal/mol. Version 2 of ANI was recently reported and showed to achieve errors in total energies prediction equal to 0.14 kcal/mol [13]. A deep tensor NN (DTNN) to mimic many-body Hamiltonians was proposed in [36]. In the same study, the authors introduced continuous filter convolutional layers (called SchNet) as novel building blocks for deep NN [37]. The reported accuracy achieved by SchNet on QM9 is 0.32 kcal/mol for  $U_0$  and 0.04 eV and 0.03 eV for HOMO and LUMO energies respectively. A KRR model with a SOAP descriptor was developed in [38], a complex NN architecture called PhysNet in [14]. These approaches reached a MAE of 0.14 kcal/mol on total energies. The MatErials Graph Network (MEGNet), an implementation of DeepMind's graph networks [59] for universal ML in materials science was proposed in [44], and achieved very low prediction errors in a broad range of properties in both molecules and crystals.

The advances in accuracy achieved for energetic properties of QM9 are truly remarkable. However, much needs to be done in topics like molecular representation that captures all the features of the molecule, or in the development of new approaches for predicting a broader range of molecular properties below the acceptable chemical accuracy. Our goal in this study is to explore the MD problem from a new perspective using techniques inspired and deeply rooted into SP. The challenge is to do it within the SP framework, in a way that performs similarly or better compared to the existing state-of-the-art techniques, and also showing the advantages of using SP within the MD pipeline.

### IV. QM9 DATASET

QM9 is a comprehensive and publicly available dataset that provides geometric, energetic, electronic and thermodynamic properties for a subset of GDB-17 database, comprising 134K

stable drug-like molecules that span a wide range of organic molecules. Molecules in the dataset consist of Hydrogen (H), Carbon (C), Oxygen (O), Nitrogen (N), and Fluorine (F) atoms and contain up to 9 heavy (non-Hydrogen) atoms. For each molecule DFT<sub>QM</sub> is used to find a reasonable low energy structure and hence atom “positions” are available. For example, **Fig. 1** shows an entry (gdb\_1) of the QM9 dataset, the methane (CH<sub>4</sub>) molecule. This entry describes the atomic composition of CH<sub>4</sub>, its atomic coordinates and its properties computed using DFT<sub>QM</sub>. **Fig. 2** shows a sketch of CH<sub>4</sub>, with atomic number of each atom added.

Number of atoms		19 Properties (truncated)						
ID	Atoms	X	Y	Z				
1	5							
2	gdb 1	157.7118	157.71	157.707	0	13.21		
3	C	-0.0127	1.085804	0.008001	-0.53569			
4	H	0.00215	-0.00603	0.001976	0.133921			
5	H	1.011731	1.463751	0.000277	0.133922			
6	H	-0.54082	1.447527	-0.87664	0.133923			
7	H	-0.52381	1.437933	0.906397	0.133923			

**Fig. 1.** Methane CH<sub>4</sub> molecule (gdb\_1) as taken from the QM9 dataset. In row 1, 5 is the number of atoms. In row 2 we have the ID of methane CH4 in the database, this is followed by the properties of the molecules. Only the five first properties are shown. Then row 3 to 7 and column 4 to 6 correspond to the coordinates (x, y z) of each atom.

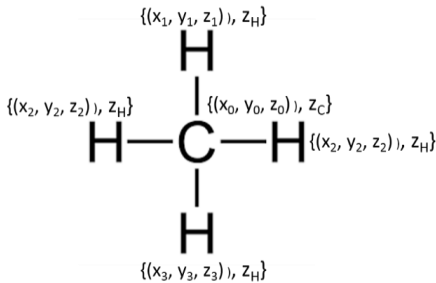


**Fig. 2.** Sketch of Methane CH<sub>4</sub> molecule (gdb 1) as taken from the QM9 dataset, the (x, y, z) represent the coordinates of the atoms, and the z the atomic number of each atom.

In addition to the geometry, a wide range of interesting and fundamental chemical properties (energetic, electronic, and thermodynamic) are computed. Given how fundamental some of the QM9 properties are, it is hard to believe that success on more challenging chemical tasks will be possible if we can't make accurate statistical predictions for the properties computed in QM9. For these reasons, the QM9 dataset has been used as a benchmark for ML algorithms [3].

The version of the QM9 dataset we used has 19 properties, available in [\[http://moleculenet.ai/datasets-1\]](http://moleculenet.ai/datasets-1). We organized them in a  $P = [p_{ml}]$  matrix, where  $p_{ml}$  is a real value that corresponds to the  $l^{\text{th}}$  property of the  $m^{\text{th}}$  molecule, with  $l = 1$  to  $L = 19$  (**Additional File 1** at <https://github.com/TABeau/QM-SP-ML>.) These properties can be grouped into four broad categories. First, we have eight properties related to how tightly bound together the atoms in a molecule are. These measure the energy required to break up the molecule at different

temperatures and pressures. They include the internal energy at 0K (U<sub>0</sub>), internal energy at 298.15K (U<sub>298</sub>), Enthalpy at 298.15K (H<sub>298</sub>), free energy at 298.15K (G<sub>298</sub>), atomization energy at 0K (U<sub>0\_atom</sub>), atomization energy at 298.15K (U<sub>298\_atom</sub>), atomization enthalpy at (H<sub>298\_atom</sub>), and free atomization free energy at 298.15K (G<sub>298\_atom</sub>). U<sub>0\_atom</sub>, U<sub>298\_atom</sub>, H<sub>298\_atom</sub> and G<sub>298\_atom</sub> are calculated from the differences between U<sub>0</sub>, U<sub>298</sub>, H<sub>298</sub>, and G<sub>298</sub>, and the sum of reference energies of all atoms in the molecules respectively. Next there are properties related to fundamental vibrations of the molecule the zero point vibrational energy (ZPVE). Additionally, there are a number of properties that concern the states of the electrons in the molecule. They include the energy of the electron in the highest occupied molecular orbital (HOMO), the energy of the lowest unoccupied molecular orbital (LUMO) and the electron energy gap, which is the difference HOMO – LUMO. There are several measures of the spatial distribution of electrons in the molecule. These include the electronic spatial extent ( $r_2$ ), the norm of the dipole moment ( $\mu$ ) and the norm of static polarizability ( $\alpha$ ). Finally, we also have other properties such as the heat capacity (cv) and the rotational constants (A, B, C). For a more detailed description of these properties, see [40].

## V. COULOMB MATRIX AND 1D REPRESENTATION OF MOLECULES

One of the major challenges in QM $\leftrightarrow$ ML is how to represent molecules in a ML pipeline. In this study, our starting point is the CM representation proposed in [8].

### A. Coulomb Matrix (CM)

Given a molecule its CM is defined by:  $C = [c_{ij}]$ , with  $c_{ij}$  defined in (4).

$$c_{ij} = \begin{cases} 0.5Z_i^{2.4} & \text{for } i = j \\ \frac{Z_i Z_j}{||R_i - R_j||} & \text{for } i \neq j \end{cases} \quad (4)$$

Where  $Z_i$  is the atomic number of atom  $i$ , and  $R_i = (x_i, y_i, z_i)$  is its position in atomic units. CM is of size  $I \times I$ , where  $I$  corresponds to the number of atoms in the molecule. It is symmetric and has as many rows and columns as there are atoms in the molecule. The CM is invariant to rotation, translation but not to permutation of its atoms. Several techniques to tackle this issue have been explored in the literature. Examples include working with a sorted CM and with the Coulomb Eigen-spectrum (CES), which will be the one used in this study.

The advantage of using the CM is that, it is based on a strict first principles view of the CCS [2]. It uses  $R$  (positions) and  $Z$  (nuclear charges) the same variables that also enter the SE. Recall that the solutions to SE are inferred for molecules using the same variables that also enter the electronic Hamiltonian  $H$ , and that are mapped to the corresponding total potential energy,  $H(\{Z, R\}) \xrightarrow{\psi} E$  [11, 12]. Unlike other QSPR representations, this ML model is free of any heuristics and it exactly encodes the supervised learning problem posed by SE. In other

words, instead of finding the wavefunction  $\Psi$  which maps the system's Hamiltonian to its energy (as one will do in QM), the ML approach directly maps the system to energy (based on examples given for training),  $\{Z, R\} \xrightarrow{ML} E$ . For this reason, this constitutes a well-defined supervised learning problem. When the number of training examples tends to a large number or infinity the ML model becomes a formally exact inductive equivalent to the deductive solution of SE.

### B. 1D Signal of Molecules - Coulomb Eigen Spectrum (CES)

Given C, the CM of a molecule, the CES is obtained by solving the Eigen value problem  $Cu = \lambda u$ , under the constraints  $\lambda_i > 0, \lambda_i \geq \lambda_{i+1}$ . The spectrum  $(\lambda_1, \dots, \lambda_l)$  which can be viewed as a 1D signal, is used as the representation of the molecule. Here, the 1D signal  $(\lambda_1, \dots, \lambda_l)$  of the  $m^{\text{th}}$  molecule ( $\Omega_m$ ) is denoted as:  $z(m, :) = z_m[n]$ , with  $n = 1$  to  $N$ . For a set of  $M$  molecules, their 1D CES signals can be organized in an  $M \times N$  matrix  $z$ :

$$z = \begin{bmatrix} z_{11} & z_{12} & \dots & z_{1n} & \dots & z_{1N} \\ z_{21} & z_{22} & \dots & z_{2n} & \dots & z_{2N} \\ \vdots & \vdots & \vdots & \vdots & \vdots & \vdots \\ z_{m1} & z_{m2} & \dots & z_{mn} & \dots & z_{mN} \\ \vdots & \vdots & \vdots & \vdots & \vdots & \vdots \\ z_{M1} & z_{M2} & \dots & z_{Mn} & \dots & z_{MN} \end{bmatrix}. \quad (5)$$

The  $m^{\text{th}}$  row of  $z$  represents the 1D signal of the  $m^{\text{th}}$  molecule. Since molecules have different number of atoms, the size of the matrix will be determined by the molecule with the largest number of atoms. Accordingly, matrices corresponding to shorter molecules will be padded with zeros all of the 1D signals will then have the same length  $N$ .

## VI. TIME FREQUENCY REPRESENTATION OF MOLECULES

Time frequency representations are widely used in SP to represent, visualize and analyze signals. Here, we explore these representations in the context of MD as input to a ML framework and draw hypotheses on their usefulness in molecular forward and inverse design. These transforms are referred to in this study as the time-frequency-like (TFL) transform. They do not have a time component like a typical 1D signal, but their elements form a totally ordered set (in this case the sorted eigenvalues. Note that magnitudes varying on a transect along the distance from a starting point defines 1D signals in many domains.) This study tests the short time Fourier transform, the continuous wavelet transform and the Wigner-Ville distribution.

### A. Discrete Fourier Transform (DFT<sub>SP</sub>)

Given the 1D signal  $z_m[n]$  of the  $m^{\text{th}}$  molecule with length  $N$ , its DFT<sub>SP</sub> is another sequence  $Z_m[k]$  of the same length  $N$  ( $k = 0$  to  $N-1$ ) given by

$$Z_m(k) = \sum_{n=0}^{N-1} z_m(n) e^{-j \frac{2\pi k n}{N}} \quad (6)$$

This transformation provides a measure of the frequency content at frequency  $k$ , which corresponds to an underlying period of  $N/k$  samples, where the maximum frequency

corresponds to  $k = N/2$ , assuming that  $N$  is even.

### B. Short Time Discrete Fourier Transform and Spectrogram

The short time Fourier transform (STFT) of  $z_m[n]$  is obtained by applying the DFT<sub>SP</sub> over a sliding window of small width to a long sequence.

$$S_{z_m(n)}(k, w) = \sum_{n=0}^{N-1} z_m(n) w(n - q) \exp\left(-\frac{j2\pi k n}{N}\right) \quad (7)$$

$$\text{Spectrogram}(z_m(n)) = |S_{z_m(n)}(k, w)|^2 \quad (8)$$

This equation provides a localized measure of the frequency content of  $z_m[n]$ . The squared magnitude of the STFT (Eq. 8) yields the spectrogram, which is a representation of the power spectral density of the function.

### C. Continuous Wavelet Transform and Scalogram

The continuous wavelet transform (CWT) of the 1D signal  $z_m(t = n)$ , at a scale ( $a > 0$ )  $a \in R^{+*}$  and translational  $b \in R$  value is defined by:

$$Z_{cwt}(a, b) = \frac{1}{\sqrt{|a|}} \int_{-\infty}^{+\infty} Z_m(t) \bar{\Psi}\left(\frac{t-b}{a}\right) dt \quad (9)$$

$\Psi(t)$  is a continuous function in the time and frequency domain called the mother wavelet. The mother wavelet provides a source function that generate daughter wavelets which are simply the translated and scaled version of the mother wavelet.

$$\text{Scalogram}(z_m(t)) = |Z_{cwt}(a, w)| \quad (10)$$

The scalogram is the absolute value of the CWT of  $z_m[t]$ , plotted as a function of time and frequency.

### D. Wigner-Ville Distributions

The Wigner-Ville distribution (WVD) provides a high-resolution time-frequency representation of a signal. For a continuous signal  $z_m(t)$ , the Wigner-Ville distribution is defined as:

$$WVD_{z_m}(t, f) = \int_{-\infty}^{+\infty} z_m(t + \frac{\tau}{2}) z_m^*(t - \frac{\tau}{2}) e^{-j2\pi f \tau} d\tau \quad (11)$$

For a discrete signal with  $N$  samples, the distribution becomes

$$WVD_{z_m}(n, k) = \sum_{q=-N}^N z_m(n + \frac{q}{2}) z_m^*(n - \frac{q}{2}) e^{-j2\pi k q / N} \quad (12)$$

For odd values of  $m$ , the definition requires evaluation of the signal at half-integer sample values. It therefore requires interpolation, which makes it necessary to zero-pad the DFT<sub>SP</sub> to avoid aliasing.

## VII. LEARNING THE MAPPING BETWEEN TIME FREQUENCY REPRESENTATION AND PROPERTIES OF MOLECULES: (DEEP) CONVOLUTIONAL NEURAL NETWORKS

In the solution of the direct problem, molecules are modeled using their TFL representations defined above. They correspond to the input of the system, while the properties

correspond to its output. The objective is to learn a mapping (i.e. infer the function  $f(\cdot)$ ) between the TFL representation (2D images) of a molecule and their properties (scalar). From a mathematical and ML perspective, this is a regression problem and it is tackled here using (deep) convolutional neural networks (CNNs).

Deep CNNs are computational architectures introduced in [60]. They have been shown to deliver remarkable regression and classification results in high dimension [61]-[62]. CNNs iterate over linear operators  $W_j$  including convolutions, and predefined pointwise nonlinearities. A CNN takes as input a tensor (In the present study it will be a 2D tensor transformed as an image containing the TFL representation.)  $x(u)$ . An internal network layer  $x_j(u, k_j)$  at a depth  $j$  is indexed by the same translation variable  $u$ , usually subsampled and a channel index  $k_j$ . A layer  $x_j$  is computed from  $x_{j-1}$  by applying a linear operator  $W_j$  followed by a pointwise nonlinearity  $\rho$ :

$$x_j = \rho W_j x_{j-1}. \quad (13)$$

The nonlinearity  $\rho$  transforms each coefficient  $\alpha$  of the array  $W_j x_{j-1}$ , and satisfies the contraction condition. A usual choice is the rectifier  $\rho(\alpha) = \max(\alpha, 0)$  for  $\alpha \in \mathbb{R}$ , but it can also be a sigmoid, or a modulus  $\rho(\alpha) = |\alpha|$  where  $\alpha$  may be complex. Because most classification and regression functions  $f(x)$  are invariant or covariant to translations, the architecture imposes that  $W_j$  is covariant to translations. The output is translated if the input is translated. Because  $W_j$  is linear, it can thus be written as a sum of convolutions:

$$W_j x_{j-1} = \sum_k \sum_v x_{j-1}(v, k) w_{j, k_j}(u - v, k) \quad (14)$$

$$W_j x_{j-1} = \sum_k (x_{j-1}(\cdot, k) * w_{j, k_j}(\cdot, k))(u) \quad (15)$$

The variable  $u$  is usually subsampled. For a fixed  $j$ , all filters  $w_{j, k_j}(u, k)$  have the same support width along  $u$ . The operators  $\rho W_j$  propagate the input signal  $x_0 = x$  until the last layer  $x_j$ . This cascade of spatial convolutions defines translation covariant operators of progressively wider supports as the depth  $j$  increases [63].

Training NNs include many side tricks, like normalizing the amplitude of  $x_j(v, k)$ , by dividing it by the norm of all coefficients  $x_j(v, k)$  for  $v$  in a neighborhood of  $u$ . This eliminates multiplicative amplitude variabilities. Instead of subsampling on a regular grid, a max pooling may select the largest coefficients over each sampling cell. Coefficients may also be modified by subtracting a constant adapted to each coefficient. When applying a rectifier  $\rho$ , this constant acts as a soft threshold, which increases sparsity.

The deep network output  $x_j = \Phi_j(x)$  is usually composed of fully connected NN layers [60]. Supervised deep learning algorithms optimize the filter values  $w_j, k_j(u, k)$  in order to minimize the average classification or regression error on the training samples  $\{x_i, f(x_i)\} i \leq q$ . The filter update is done with a back-propagation algorithm, which may be computed with the adaptive moment estimation (Adam), a stochastic gradient descent (SGD), with regularization procedures such as dropout. These high-dimensional optimizations are non-convex, but

despite the presence of many local minima, the regularized converges to a local minimum providing good accuracy on test examples [63].

## VIII. RESULTS AND DISCUSSIONS

The CES of each molecule was computed using their atomic coordinates as described in the QM9 dataset and the approach described above. They were then organized in an  $M \times N = 133885 \times 29$  matrix (**Additional File 2** at <https://github.com/TABeau/QM-SP-ML>).  $M = 133885$  corresponds to the number of molecules in the QM9 dataset and  $N = 29$  the number of atoms in the largest molecule. As mentioned in Section V, molecules with less than 29 atoms were padded with zeros so that all the 1D signals have the same dimension ( $N = 29$ ). The STFT used a Hamming window, the CWT a Morlet (Gabor) wavelet, and the WVD of each molecule was computed using the Matlab script provided as **Additional File 3** at <https://github.com/TABeau/QM-SP-ML>. As an example, **Fig. 3** illustrates the case of molecule  $C_3H_7NO$  (ID = gdb\_49 in the QM9 dataset). (A) is the molecule, (B) its 1D signal according to the aforementioned representation procedure, (C) the amplitude of its 1D DFT<sub>SP</sub>, (D) its Spectrogram, (E) its Scalogram and (F) its WVD, respectively.

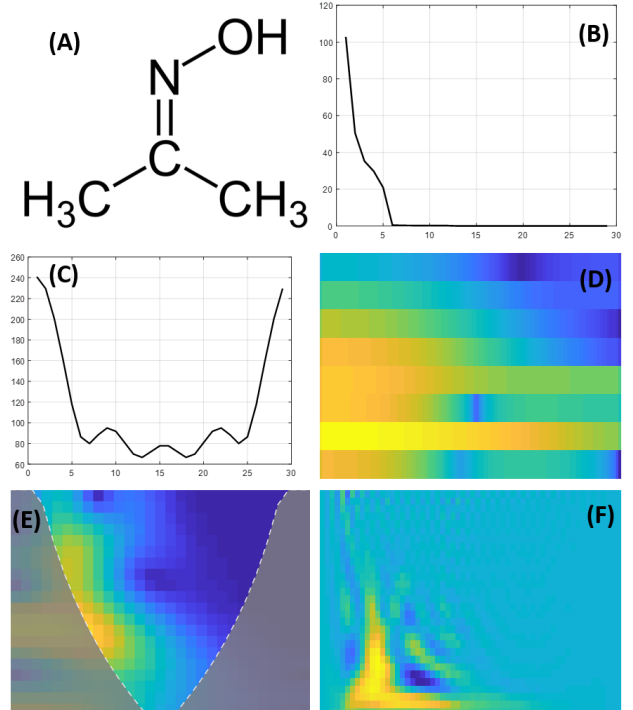


**Fig. 3.** (A) Chemical representation of molecule ID gdb\_49 in the QM9 dataset which corresponds to one of the isomers of  $C_3H_7NO$ , (B) its 1D signal, (C) the amplitude of its discrete Fourier transform, (D) its Spectrogram (amplitude of its STFT), (E) its Scalogram (CWT) and (D) its Wigner-Ville Distribution (WVD).

The dataset was randomly divided into 90% (120 500  $\approx$  120K) for training and the remaining 10% (13 389  $\approx$  13K) for testing. A deep CNNs was constructed using the Python script provided as **Additional File 4** at <https://github.com/TABeau/QM-SP-ML>. Readers can refer to

this file for details relative to the construction of the deep CNNs. Training of each TFL representation was performed on three different machines with GPU (NVIDIA Quadro K2200, NVIDIA Quadro P2000, NVIDIA GeForce GTX TITAN X) capabilities and took 3, 2 to 1 weeks for completion respectively. Performance of the  $n^{\text{th}}$  property is measured using the mean absolute error (MAE)

$$MAE_n = \frac{1}{M} \sum_{m=1}^M |P_{mn} - P_{mn}^e| . \quad (16)$$

$P_{mn}$  is the measured  $n^{\text{th}}$  property of the  $m^{\text{th}}$  molecule, and  $P_{mn}^e$  the estimated one.

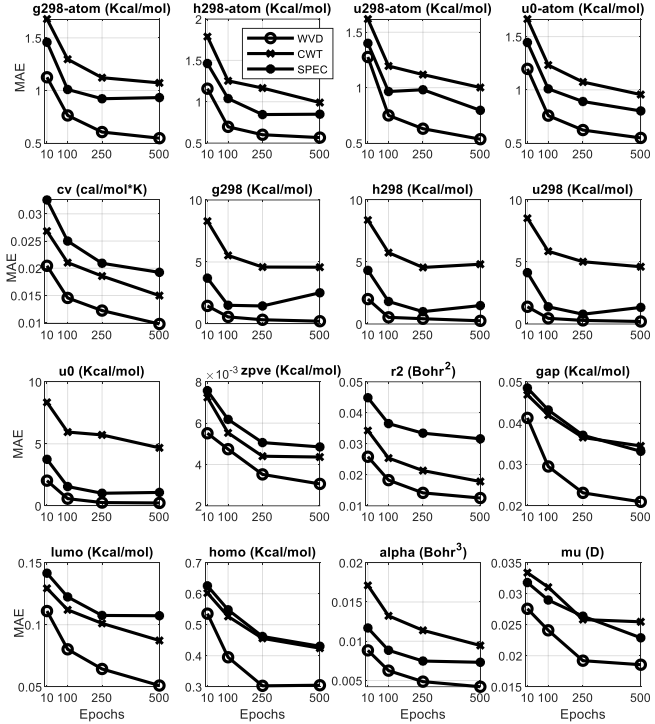


**Fig. 4.** MAE evolution of 16 out of 19 properties, vs. number of epochs for each time-frequency like representation during the training stage. The Y-axis correspond to the MAEs and the X-axis to the number of epochs.

**Fig. 4** and **Fig. 5** show the training and testing results obtained for 10, 100, 250, and 500 epochs for 16 out of the 19 properties, for WVD, CWT and STFT respectively. The best results for each TFL representation (i.e. the MAE obtained prior to the model starts overfitting) are presented in **Table III**. It is interesting to note that several of these properties are predicted with MAE below chemical accuracy.

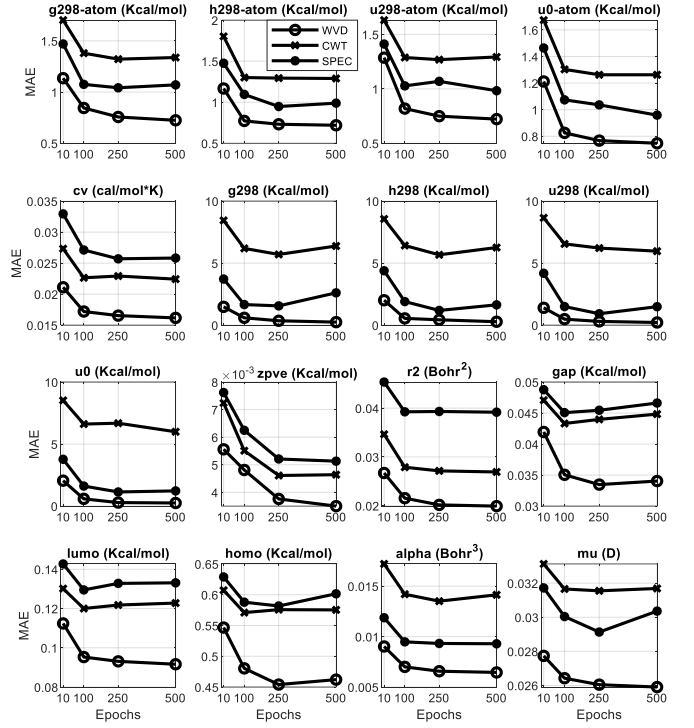


**Fig. 5.** MAE evolution of the 16 out of 19 properties, with number of epochs for each time-frequency-like representations during the testing stage. The Y-axis correspond to the MAEs and the X-axis to the number of epochs.

**TABLE III**  
MEAN ABSOLUTE ERRORS OF THE THREE REPRESENTATIONS ON THE TESTING SET.

Properties	Unit	MAE			Epochs
		STFT	CWT	WVD	
g298_atom	kcal/mol	1.042	1.321	0.724	[250 250 500]
h298_atom	kcal/mol	0.948	1.294	0.719	[250 250 500]
u298_atom	kcal/mol	0.982	1.292	0.722	[500 250 500]
u0_atom	kcal/mol	0.958	1.262	0.747	[500 500 500]
cv	cal/(mol*K)	0.025	0.022	0.016	[500 500 500]
g298	kcal/mol	1.554	5.701	0.244	[250 250 500]
h298	kcal/mol	1.186	5.671	0.277	[250 250 500]
u298	kcal/mol	0.921	6.214	0.216	[250 500 500]
u0	kcal/mol	1.141	6.684	0.251	[250 500 500]
zpve	kcal/mol	0.005	0.004	0.003	[500 250 500]
r2	Bohr^2	0.039	0.026	0.019	[500 500 500]
gap	kcal/mol	0.045	0.043	0.033	[100 100 250]
lumo	kcal/mol	0.129	0.120	0.091	[100 100 500]
homo	kcal/mol	0.581	0.570	0.454	[250 100 250]
alpha	Bohr^3	0.009	0.013	0.006	[500 250 500]
mu	D	0.029	0.031	0.025	[250 250 500]
C	GHz	-	-	-	-
B	GHz	-	-	-	-
A	GHz	-	-	-	-

The epochs column = [STFT CWT WVD] specifies the number of epochs where each representation achieved the best MAE result respectively, prior to the model starts overfitting.

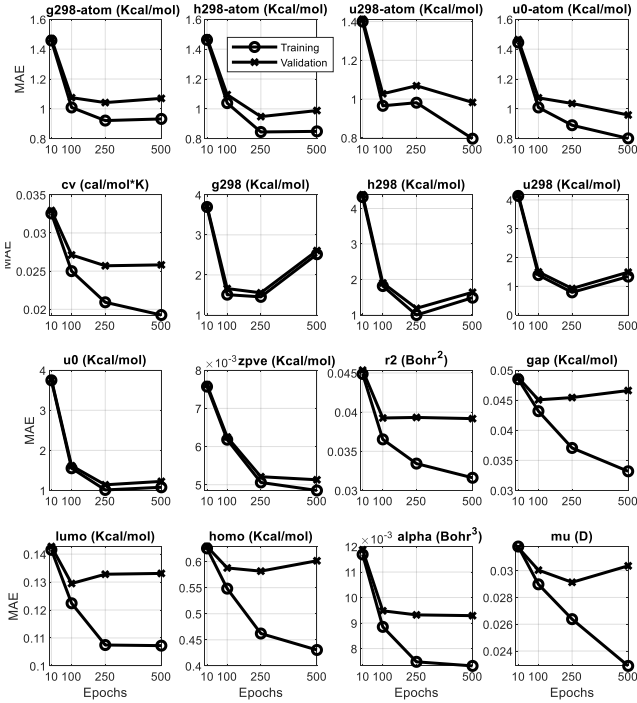


**Fig. 6.** MAE evolution of the 16 out of 19 properties, with number of epochs for the STFT/Spectrogram during the training and testing stage. The Y-axis correspond to the MAEs and the X-axis to the number of epochs.

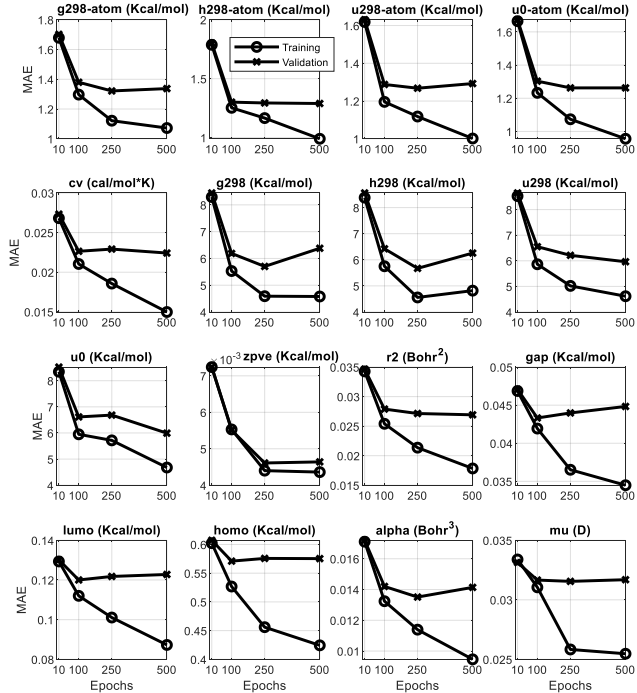


**Fig. 7.** MAE evolution of the 16 out of 19 properties, with number of epochs for the Scalogram/continuous wavelet transform during the training and testing stage. The Y-axis correspond to the MAEs and the X-axis to the number of epochs.

**Fig. 6, Fig. 7 and Fig. 8** shows the combined MAE evolution of training and testing for STFT, CWT and WVD on the same graph respectively. These figures show a better description of when the corresponding model starts overfitting. For example, for the LUMO property, the model corresponding to the STFT and CWT representations start to overfit after 100 epochs,

whereas the one corresponding to WVD keeps improving up to 500 epochs.

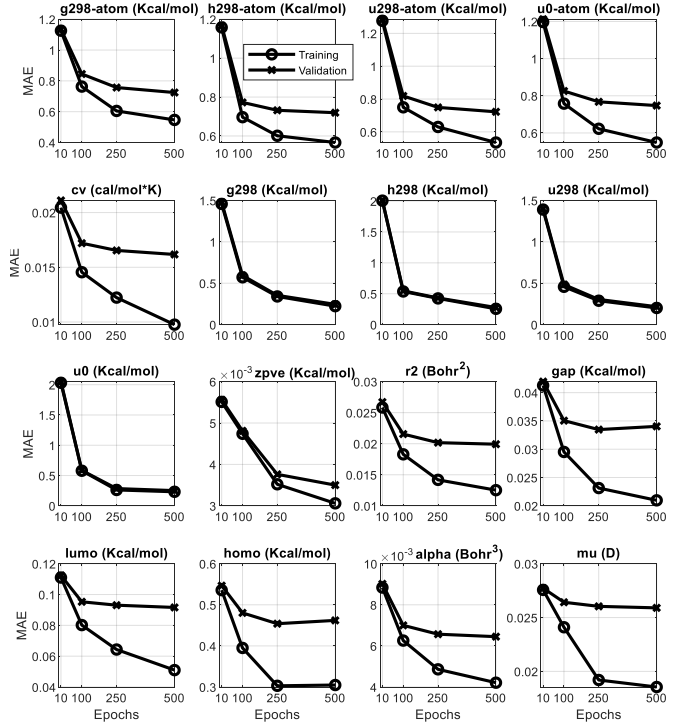


**Fig. 8.** MAE evolution of the 16 out of 19 properties, with number of epochs for the Wigner-Ville Distribution (WVD) during the training and testing stage. The Y-axis correspond to the MAEs and the X-axis to the number of epochs.

#### A. Comparison between STFT, CWT, and WVD

Among the three representations, the model relative to the WVD gave the best training and testing set prediction results for all the 19 properties and for models at 10, 100, 250 and 500 epochs compared to the STFT and CWT. The STFT came second and the CWT third. More precisely, the WVD predicted 16 properties out of 19 with MAEs bellow chemical accuracy. The STFT predicted 16 out of 19 with 12 MAEs below chemical accuracy and 4 equal or slightly above chemical accuracy. The CWT performed the worst. It predicted 16 out of 19 properties with only 8 properties below chemical accuracy.

#### B. Comparison between $QM \leftrightarrow SP \leftrightarrow ML$ and other ML Techniques

**Table IV** gives a comparative analysis of the  $QM \leftrightarrow SP \leftrightarrow ML$  method and the state-of-the-art ML techniques described in the literature and mentioned in **Table II** above. On the  $G_{298\_atom}$ ,  $H_{298\_atom}$ ,  $U_{298\_atom}$  and  $U_0\_atom$ , the WVD scored a MAE of around 0.7 Kcal/mol, which is  $< 1$  Kcal/mol. There were no other available ML results in the literature for comparison. On the  $G_{298}$ ,  $H_{298}$ , and  $U_{298}$ , our approach via the WVD was slightly better compared to the results mentioned in the literature. We obtained MAEs of 0.244Kcal/mol, 0.277Kcal/mol, 0.216Kcal/mol compared to 0.276 Kcal/mol, 0.276Kcal/mol and 0.299Kcal/mol of the MEGNet algorithm respectively. On the  $U_0$ , among the six ML approaches that we compared the  $QM \leftrightarrow SP \leftrightarrow ML$  to, the WVD came second with a MAE of 0.25 Kcal/mol slightly higher than the 0.14Kcal/mol obtained by the SOAP algorithm [38] and the PhysNet algorithm [14].

**TABLE IV**

MAE VALUES ON THE TESTING SET OF THE COMPARATIVE ANALYSIS OF THE  $QM \leftrightarrow SP \leftrightarrow ML$  APPROACH WITH STATE-OF-THE-ART ML TECHNIQUES FOR THE 19 PROPERTIES OF THE QM9 DATASET.

Properties	Units	QM-SP-ML	MEGNet	KRR/BAML	GPR/SOAP/GAP	NMP	Multitask	SchNet	HIP-NN	HDNN	KRR/SOAP	PhysNet
g298_atom	kcal/mol	<b>0.724</b>	-	-	-	-	-	-	-	-	-	-
h298_atom	kcal/mol	<b>0.719</b>	-	-	-	-	-	-	-	-	-	-
u298_atom	kcal/mol	<b>0.722</b>	-	-	-	-	-	-	-	-	-	-
u0_atom	kcal/mol	<b>0.747</b>	-	-	-	-	-	-	-	-	-	-
cv	cal/(mol*K)	<b>0.016</b>	0.029	1.64	-	0.80	0.124	0.033	-	-	-	-
g298	kcal/mol	<b>0.244</b>	0.276	1.20	-	0.44	44.32	0.322	-	-	-	-
h298	kcal/mol	<b>0.277</b>	<b>0.276</b>	1.22	-	0.39	44.16	0.322	-	-	-	-
u298	kcal/mol	<b>0.216</b>	0.299	1.22	-	0.45	43.96	0.438	-	-	-	-
u0	kcal/mol	0.251	0.276	1.21	0.28	0.45	44.04	0.32	0.26	0.41	<b>0.14</b>	<b>0.14</b>
zpve	kcal/mol	3e-3	<b>3e-5</b>	3.31	-	1.27	0.199	<b>3e-5</b>	-	-	-	-
r2	Bohr^2	<b>0.019</b>	0.302	3.25	-	0.15	2.056	0.073	-	-	-	-
gap	kcal/mol	<b>0.033</b>	1.522	3.28	-	1.60	2.014	1.452	-	-	-	-
lumo	kcal/mol	<b>0.091</b>	1.014	2.76	-	0.87	1.133	0.691	-	-	-	-
homo	kcal/mol	<b>0.454</b>	0.991	2.20	-	0.99	1.620	0.922	-	-	-	-
alpha	Bohr^3	<b>0.006</b>	0.081	3.01	-	0.92	0.571	0.235	-	-	-	-
mu	D	<b>0.025</b>	0.050	4.34	-	0.30	0.304	0.033	-	-	-	-
C	GHz	-	-	-	-	-	0.009	-	-	-	-	-
B	GHz	-	-	-	-	-	0.016	-	-	-	-	-
A	GHz	-	-	-	-	-	0.099	-	-	-	-	-

On the zpve, our approach score a MAE of 3e-3Kcal/mol and came third compared to the 3e-5Kcal/mol of MEGNet and SchNet. On cv,  $r_2$ , gap, LUMO, HOMO, alpha and mu properties, our three representations (STFT, CWT, and WVD) gave better results compared to the ones mentioned in the literature. Finally, on the C (rotational constant), B (rotational constant) and A (rotational constant) our methods failed to predict compared to the MAEs of 0.009, 0.016, 0.099 GHz obtained by the multitask NN algorithm [33].

In all the new proposed  $QM \leftrightarrow SP \leftrightarrow ML$  model via the WVD representation outperforms several of the state-of-the-art ML techniques described in the literature on the prediction of 14 properties and was able to predict 16 out of 19 properties of the QM9 dataset with MAEs below chemical accuracy.

### C. What Information are Encoded in the Time-Frequency Representations?

The success of the TFL representations of molecules in the prediction of their properties with MAEs below chemical accuracy mean that these representations encode very relevant information pertaining to the molecules. The connection between the TFL representations and the structure of the molecule is obvious because the TFL representations are inferred from the CM which are computed using the atomic coordinates. Note that the CM is directly derived from the geometry representation of molecules. It is well known that the structure of a molecule dictates its properties. This structure to property relationship combined with the fact that the TFL representations are able to predict the properties of molecules with MAEs below chemical accuracy further validate the fact that chemical knowledge is indeed encoded in them. Another question that might come up is, why not just use the 1D signal representation (i.e. CES) and not the TFL representation as input to ML framework? Why taking this extra step to convert the 1D numerical signal to a 2D image signal? The Multitask NN algorithm [33] did just that. In the multitask NN the 1D CES representation of molecule is used as input to a deep multitask NN. As we showed in this study (**Table IV**), the new  $QM \leftrightarrow SP \leftrightarrow ML$  model based on image representation

outperformed the multitask NN on 16 properties out of 19. For example our algorithm predicted  $G_{298}$ ,  $H_{298}$ ,  $U_{298}$ , and  $U_0$  with MAEs below chemical accuracy whereas the multitask NN scored  $\sim 44$ Kcal/mol, way above chemical accuracy. This is a very big difference and further validate the extra step of converting the 1D signal into a 2D representation. The fact that the TFL representations perform better than the 1D CES suggests that information that were not obvious in the 1D signal are amplified and made explicit in the 2D image representations. In audio SP for example, it is well known that the appearance of spectrograms provides significant information about signals, to the extent that trained observers can figure out the words uttered in voice signals by simple visual inspection of their spectrograms [46].

## IX. CONCLUSIONS

Materials are generally defined by the atoms that make them, and the structures and compositions that these atoms take up. Properties of materials such as color, hardness, conductivity, stability, topology or magnetism exist in certain substances and not others. The question is how can we find materials with just the right properties we dream of? In this study, we showed that time-frequency-*like* representations of molecules is a powerful tool that can be used for molecular representation and visualization. We demonstrated that these representations encode the structural, geometric, energetic, electronic and thermodynamic properties of molecules. Using a deep convolutional neural networks approach in a regression framework and the benchmark QM9 dataset, we showed that there exist a clear relationship between the time-frequency-*like* representations and the structure, energetic, electronic, and thermodynamic properties of the molecules. All the codes and data generated and used in this study are available at <https://github.com/TABeau/QM-SP-ML>. **Additional File 5** contains the Molecules ID. The readme file contains a detail description of all the additional files and how to set the Matlab codes, Python scripts, and different files and folders to run on a

computer.

## ACKNOWLEDGMENT

This work is supported by the National Research Council of Canada through its Artificial Intelligence for Design Program led by the Digital Technologies Research Centre.

## REFERENCES

- [1] G. Montavon, M. Rupp, V. Gobre, A. Vazquez-Mayagoitia, K. Hansen, A. Tkatchenko, K.-R. Müller, and O. A. V. Lilienfeld, “Machine learning of molecular electronic properties in chemical compound space,” *New Journal of Physics*, vol. 15, no. 9, p. 095003, Apr. 2013.
- [2] G. Montavon, K. Hansen, S. Fazli, M. Rupp, F. Biegler, A. Ziehe, A. Tkatchenko, O. A. Von Lilienfeld, K.-R. Müller, “Learning invariant representations of molecules for atomization energy prediction,” In *Proceedings of the 25th International Conference on Neural Information Processing Systems*, vol. 1, P. 440-448, 2012.
- [3] M. Glavatskikh, J. Leguy, G. Hunault, T. Cauchy, and B. D. Mota, “Dataset’s chemical diversity limits the generalizability of machine learning predictions,” *Journal of Cheminformatics*, vol. 11, no. 1, Dec. 2019.
- [4] L. C. Blum and J.-L. Reymond, “970 Million Druglike Small Molecules for Virtual Screening in the Chemical Universe Database GDB-13,” *Journal of the American Chemical Society*, vol. 131, no. 25, pp. 8732–8733, 2009.
- [5] Y. Wang, J. Xiao, T. O. Suzek, J. Zhang, J. Wang, and S. H. Bryant, “PubChem: a public information system for analyzing bioactivities of small molecules,” *Nucleic Acids Research*, vol. 37, no. Web Server, Apr. 2009.
- [6] M. Nakata and T. Shimazaki, “PubChemQC Project: A Large-Scale First-Principles Electronic Structure Database for Data-Driven Chemistry,” *Journal of Chemical Information and Modeling*, vol. 57, no. 6, pp. 1300–1308, 2017.
- [7] S. Kim, J. Chen, T. Cheng, A. Gindulyte, J. He, S. He, Q. Li, B. A. Shoemaker, P. A. Thiessen, B. Yu, L. Zaslavsky, J. Zhang, and E. E. Bolton, “PubChem 2019 update: improved access to chemical data,” *Nucleic Acids Research*, vol. 47, no. D1, 2018.
- [8] M. Rupp, A. Tkatchenko, K.-R. Müller, and O. A. V. Lilienfeld, “Fast and Accurate Modeling of Molecular Atomization Energies with Machine Learning,” *Physical Review Letters*, vol. 108, no. 5, 2012.
- [9] M. Rupp, “Machine learning for quantum mechanics in a nutshell,” *International Journal of Quantum Chemistry*, vol. 115, no. 16, pp. 1058–1073, Apr. 2015.
- [10] D. Xue, P. V. Balachandran, J. Hogden, J. Theiler, D. Xue, and T. Lookman, “Accelerated search for materials with targeted properties by adaptive design,” *Nature Communications*, vol. 7, no. 1, 2016.
- [11] K. Hansen, F. Biegler, R. Ramakrishnan, W. Pronobis, O. A. V. Lilienfeld, K.-R. Müller, and A. Tkatchenko, “Machine Learning Predictions of Molecular Properties: Accurate Many-Body Potentials and Nonlocality in Chemical Space,” *The Journal of Physical Chemistry Letters*, vol. 6, no. 12, pp. 2326–2331, Oct. 2015.
- [12] K. Hansen, G. Montavon, F. Biegler, S. Fazli, M. Rupp, M. Scheffler, O. A. V. Lilienfeld, A. Tkatchenko, and K.-R. Müller, “Assessment and Validation of Machine Learning Methods for Predicting Molecular Atomization Energies,” *Journal of Chemical Theory and Computation*, vol. 9, no. 8, pp. 3404–3419, 2013.
- [13] J. S. Smith, B. T. Nebgen, R. Zubatyuk, N. Lubbers, C. Devereux, K. Barros, S. Tretiak, O. Isayev, and A. E. Roitberg, “Approaching coupled cluster accuracy with a general-purpose neural network potential through transfer learning,” *Nature Communications*, vol. 10, no. 1, Jan. 2019.
- [14] O. T. Unke and M. Meuwly, “PhysNet: A Neural Network for Predicting Energies, Forces, Dipole Moments, and Partial Charges,” *Journal of Chemical Theory and Computation*, vol. 15, no. 6, pp. 3678–3693, 2019.
- [15] D. M. Wilkins, A. Grisafi, Y. Yang, K. U. Lao, R. A. Distasio, and M. Ceriotti, “Accurate molecular polarizabilities with coupled cluster theory and machine learning,” *Proceedings of the National Academy of Sciences*, vol. 116, no. 9, pp. 3401–3406, Jul. 2019.
- [16] E. Iype and S. Urolagin, “Machine learning model for non-equilibrium structures and energies of simple molecules,” *The Journal of Chemical Physics*, vol. 150, no. 2, p. 024307, 2019.
- [17] C. Duan, J. P. Janet, F. Liu, A. Nandy, and H. J. Kulik, “Learning from Failure: Predicting Electronic Structure Calculation Outcomes with Machine Learning Models,” *Journal of Chemical Theory and Computation*, vol. 15, no. 4, pp. 2331–2345, Dec. 2019.
- [18] A. Grisafi, A. Fabrizio, B. Meyer, D. M. Wilkins, C. Corminboeuf, and M. Ceriotti, “Transferable Machine-Learning Model of the Electron Density,” *ACS Central Science*, vol. 5, no. 1, pp. 57–64, 2018.
- [19] Y. Okamoto, “Data sampling scheme for reproducing energies along reaction coordinates in high-dimensional neural network potentials,” *The Journal of Chemical Physics*, vol. 150, no. 13, p. 134103, Jul. 2019.
- [20] A. Chandrasekaran, D. Kamal, R. Batra, C. Kim, L. Chen, R. Ramprasad, “Solving the electronic structure problem with machine learning,” *NPJ Comput Mater*, vol. 5(1):22, 2019.
- [21] S. Amabilino, L. A. Bratholm, S. J. Bennie, A. C. Vaucher, M. Reiher, and D. R. Glowacki, “Training Neural Nets To Learn Reactive Potential Energy Surfaces Using Interactive Quantum Chemistry in Virtual Reality,” *The Journal of Physical Chemistry A*, vol. 123, no. 20, pp. 4486–4499, 2019.
- [22] L. Cheng, M. Welborn, A. S. Christensen, and T. F. Miller, “A universal density matrix functional from molecular orbital-based machine learning: Transferability across organic molecules,” *The Journal of Chemical Physics*, vol. 150, no. 13, p. 131103, Jul. 2019.
- [23] K. Ghosh, A. Stuke, M. Todorović, P. B. Jørgensen, M. N. Schmidt, A. Vehtari, and P. Rinke, “Deep Learning Spectroscopy: Neural Networks for Molecular Excitation Spectra,” *Advanced Science*, vol. 6, no. 9, p. 1801367, 2019.
- [24] B. Huang and O. A. V. Lilienfeld, “Communication: Understanding molecular representations in machine learning: The role of uniqueness and target similarity,” *The Journal of Chemical Physics*, vol. 145, no. 16, p. 161102, 2016.
- [25] F. A. Faber, L. Hutchison, B. Huang, J. Gilmer, S. S. Schoenholz, G. E. Dahl, O. Vinyals, S. Kearnes, P. F. Riley, and O. A. V. Lilienfeld, “Prediction Errors of Molecular Machine Learning Models Lower than Hybrid DFT Error,” *Journal of Chemical Theory and Computation*, vol. 13, no. 11, pp. 5255–5264, Oct. 2017.
- [26] C. R. Collins, G. J. Gordon, O. A. V. Lilienfeld, and D. J. Yaron, “Constant size descriptors for accurate machine learning models of molecular properties,” *The Journal of Chemical Physics*, vol. 148, no. 24, p. 241718, 2018.
- [27] A. P. Bartók, S. De, C. Poelking, N. Bernstein, J. R. Kermode, G. Csányi, M. Ceriotti, “Machine learning unifies the modeling of materials and molecules,” *Sci Adv*, vol. 3(12):1701816, 2017.
- [28] F. Pereira, K. Xiao, D. A. R. S. Latino, C. Wu, Q. Zhang, and J. Aires-De-Sousa, “Machine Learning Methods to Predict Density Functional Theory B3LYP Energies of HOMO and LUMO Orbitals,” *Journal of Chemical Information and Modeling*, vol. 57, no. 1, pp. 11–21, 2016.
- [29] J. S. Smith, O. Isayev, and A. E. Roitberg, “ANI-1: an extensible neural network potential with DFT accuracy at force field computational cost,” *Chemical Science*, vol. 8, no. 4, pp. 3192–3203, 2017.
- [30] J. Gilmer, S. S. Schoenholz, P. F. Riley, O. Vinyals, G. E. Dahl, “Neural message passing for quantum chemistry,” *arXiv:1704.01212*, 2017.
- [31] K. T. Schütt, H. E. Sauceda, P.-J. Kindermans, A. Tkatchenko, and K.-R. Müller, “SchNet – A deep learning architecture for molecules and materials,” *The Journal of Chemical Physics*, vol. 148, no. 24, p. 241722, 2018.
- [32] T. S. Hy, S. Trivedi, H. Pan, B. M. Anderson, and R. Kondor, “Predicting molecular properties with covariant compositional networks,” *The Journal of Chemical Physics*, vol. 148, no. 24, p. 241745, 2018.
- [33] F. Hou, Z. Wu, Z. Hu, Z. Xiao, L. Wang, X. Zhang, and G. Li, “Comparison Study on the Prediction of Multiple Molecular Properties by Various Neural Networks,” *The Journal of Physical Chemistry A*, vol. 122, no. 46, pp. 9128–9134, Apr. 2018.
- [34] N. Lubbers, J. S. Smith, and K. Barros, “Hierarchical modeling of molecular energies using a deep neural network,” *The Journal of Chemical Physics*, vol. 148, no. 24, p. 241715, 2018.
- [35] O. T. Unke and M. Meuwly, “A reactive, scalable, and transferable model for molecular energies from a neural network approach based on local information,” *The Journal of Chemical Physics*, vol. 148, no. 24, p. 241708, 2018.
- [36] K. T. Schütt, F. Arbabzadah, S. Chmiela, K. R. Müller, and A. Tkatchenko, “Quantum-chemical insights from deep tensor neural networks,” *Nature Communications*, vol. 8, no. 1, Sep. 2017.
- [37] K. T. Schütt, P. -J. Kindermans, H. E. Sauceda, S. Chmiela, A. Tkatchenko, K. -R. Müller, “SchNet: A continuous-filter convolutional

neural network for modeling quantum interactions," arXiv :1706.08566, 2017.

[38] M. J. Willatt, F. Musil, and M. Ceriotti, "Feature optimization for atomistic machine learning yields a data-driven construction of the periodic table of the elements," *Physical Chemistry Chemical Physics*, vol. 20, no. 47, pp. 29661–29668, 2018.

[39] F. A. Faber, A. S. Christensen, B. Huang, and O. A. V. Lilienfeld, "Alchemical and structural distribution based representation for universal quantum machine learning," *The Journal of Chemical Physics*, vol. 148, no. 24, p. 241717, 2018.

[40] R. Ramakrishnan, P. O. Dral, M. Rupp, and O. A. V. Lilienfeld, "Quantum chemistry structures and properties of 134 kilo molecules," *Scientific Data*, vol. 1, no. 1, May 2014.

[41] A. B. Tchagang and J. J. Valdés, "Discrete Fourier Transform Improves the Prediction of the Electronic Properties of Molecules in Quantum Machine Learning," *2019 IEEE Canadian Conference of Electrical and Computer Engineering (CCECE)*, 2019.

[42] A. B. Tchagang and J. J. Valdés, "Prediction of the Atomization Energy of Molecules Using Coulomb Matrix and Atomic Composition in a Bayesian Regularized Neural Networks," *Artificial Neural Networks and Machine Learning – ICANN 2019: Workshop and Special Sessions Lecture Notes in Computer Science*, pp. 793–803, 2019.

[43] J. J. Valdés and A. B. Tchagang, "Characterization of Quantum Derived Electronic Properties of Molecules: A Computational Intelligence Approach," *Artificial Neural Networks and Machine Learning – ICANN 2019: Workshop and Special Sessions Lecture Notes in Computer Science*, pp. 771–782, 2019.

[44] C. Chen, W. Ye, Y. Zuo, C. Zheng, and S. P. Ong, "Graph Networks as a Universal Machine Learning Framework for Molecules and Crystals," *Chemistry of Materials*, vol. 31, no. 9, pp. 3564–3572, Oct. 2019.

[45] B. Horst, "Molecular Descriptors and the Electronic Structure," *Statistical Modelling of Molecular Descriptors in QSAR/QSPR*, pp. 245–292, Sep. 2012.

[46] B. Porat, *A Course in digital signal processing*. New York: John Wiley, 1997.

[47] D. J. Griffiths and D. F. Schroeter, *Introduction to quantum mechanics*. Cambridge: Cambridge University Press, 2019.

[48] P. A. M. Dirac. Quantum mechanics of many electron systems. Proceedings of the Royal Society of London. Series A, Mathematical and physical sciences, 123(792):714–733, April 6, 1929.

[49] J. G. Stamper, "A note on the treatment of quadruple excitations in configuration interaction," *Theoretica Chimica Acta*, vol. 11, no. 5, pp. 459–462, 1968.

[50] R. J. Bartlett, "Coupled-Cluster Theory: An Overview Of Recent Developments," *Modern Electronic Structure Theory Advanced Series in Physical Chemistry*, pp. 1047–1131, 1995.

[51] C. D. Sherrill and H. F. Schaefer, "The Configuration Interaction Method: Advances in Highly Correlated Approaches," *Advances in Quantum Chemistry*, pp. 143–269, 1999.

[52] C. Møller, M. S. Plesset, "Note on an approximation treatment for many-electron systems," *Phys Rev*, vol. 46(7):618, 1934.

[53] B. L. Hammond, W. A. Lester, and P. J. Reynolds, *Monte Carlo methods in ab initio quantum chemistry*. Singapore: World Scientific, 1994.

[54] C. D. Sherrill, "An introduction to Hartree-Fock molecular orbital theory," [<http://vergil.chemistry.gatech.edu/notes/hf-intro/hf-intro.pdf>], June 2000

[55] W. Kohn and L. J. Sham, "Self-Consistent Equations Including Exchange and Correlation Effects," *Physical Review*, vol. 140, no. 4A, 1965.

[56] J. C. Slater and G. F. Koster, "Simplified LCAO Method for the Periodic Potential Problem," *Physical Review*, vol. 94, no. 6, pp. 1498–1524, 1954.

[57] U. Burkert and N. L. Allinger, *Molecular mechanics*. Washington (WA): American Chemical Society, 1989.

[58] D. R. Bowler and T. Miyazaki, "O(N) methods in electronic structure calculations)," *Reposrts on Progress in Physics*, vol 75, no 3, 15 February 2012.

[59] P. W. Battaglia, J. B. Hamrick, V. Bapst, A. Sanchez-Gonzalez, V. Zambaldi, M. Malinowski, A. Tacchetti, D. Raposo, A. Santoro, R. Faulkner, et al., "Relational inductive biases, deep learning, and graph networks," arXiv:1806.01261, 2018.

[60] Y. Le Cun, B. Boser, J. Denker, D. Henderson, R. Howard, W. Hubbard, L. Jackelt, "Handwritten digit recognition with a back-propagation network," In *Advances in neural information processing systems 2* (ed. DS Touretzky), pp. 396–404. San Francisco, CA: Morgan Kaufmann, 1990.

[61] Y. Le Cun, Y. Bengio, G. Hinton, "Deep learning," *Nature*, vol. 521, p. 436–444, 2015.

[62] A. Krizhevsky, I. Sutskever, and G. E. Hinton, "ImageNet classification with deep convolutional neural networks," *Communications of the ACM*, vol. 60, no. 6, pp. 84–90, 2017.

[63] S. Mallat, "Understanding deep convolutional neural networks," *Phil. Trans. R. Soc. A* 374:20150203, 13 April 2016.